*Journal of Applied Mechanics and Technical Physics, Vol. 48, No. 2, pp. 292–302, 2007*

# PRODUCTION OF NANOMATERIALS BY VAPORIZING CERAMIC TARGETS IRRADIATED BY A MODERATE-POWER CONTINUOUS-WAVE $CO_2$ LASER

**V. N. Snytnikov, Vl. N. Snytnikov,**
**D. A. Dubov, V. I. Zaikovskii,**
**A. S. Ivanova, V. O. Stoyanovskii, and V. N. Parmon**

UDC 535.211

*The efficiency of utilization of* $CO_2$ *laser energy for vaporization of* $Al_2O_3$ *ceramics is evaluated using a mathematical model for the interaction of laser radiation with materials. It is shown that the calculated efficiency of radiation-energy utilization is not higher than* 15% *at a radiation power density of* $10^5$ W/cm$^2$ *on the target. On the experimental facility designed for the synthesis of nanopowders, a vaporization rate of* 1 g/h *was achieved for* $Al_2O_3$*, which corresponds to a* 3% *efficiency of radiation-energy utilization. The dependence of the characteristic particle size of a zirconium oxide nanopowder on helium pressure in the range of* 0.01–1.00 atm *was studied. Results of experiments on vaporization of multicomponent materials* ($LaNiO_3$ *and the Tsarev meteorite*) *are given.*

**Key words:** *laser vaporization, synthesis of nanomaterials, nanoparticles, nanopowder.*

**Introduction**. Investigation of nanomaterials is a priority research area in modern science and engineering. One of the most extensive applications of these materials has been in catalytic technologies. To accelerate the synthesis and test of samples for choosing optimal compositions of catalysts in combinatorial catalysis, it is proposed to employ methods of semiconductor technologies — simultaneous testing of a large set of materials in parallel-operating catalytic microreactors [1]. It is obvious that the methods of synthesizing such materials should be universal, effective and insensitive to the nature of the materials tested: metals, their oxides, carbides, etc. In the development of catalysts, multicomponent and high-melting materials based on oxides of aluminum, zirconium, silicon, and some other elements with incorporated metal atoms, clusters, and (or) nanoparticles are of special interest. The particle sizes of catalytically active phases, as a rule, should be in the range of 1–10 nm and have a narrow adjustable particle size distribution. In view of the requirements on the quantity of the material needed to test its functional characteristics, the capacity of the facility for the synthesis of nanomaterial should be about 1 g/h.

Electron-beam and laser methods [physical vapor deposition (PVD) methods in English terminology] of precursor vaporization in a controlled atmosphere meet the indicated requirements. Obviously, because of the high power, cost and operation expenses of typical commercial accelerator [2], they are undesirable for use as laboratory facilities for solving research problems. At the same time, investigation of the interaction of laser radiation with materials has been focused primarily on the development of technologies of hard-facing, cutting or carving and, in some cases, application of coatings [2]. It has been shown [2] that metal vaporization requires a radiation power density higher than $10^6$–$10^7$ W/cm$^2$ (depending on the wavelength). Dielectrics and semiconductors vaporize at lower power densities. Nanopowders of aluminum oxide [3, 4] and iron oxide [5] were produced using high-power commercial $CO_2$ and Nd : YAG lasers, which are unsuitable under laboratory conditions.

Boreskov Institute of Catalysis, Siberian Division, Russian Academy of Sciences, Novosibirsk 630090; snyt@catalysis.nsk.su. Translated from Prikladnaya Mekhanika i Tekhnicheskaya Fizika, Vol. 48, No. 2, pp. 172–184, March–April, 2007. Original article submitted June 22, 2005; revision submitted May 29, 2006.

 

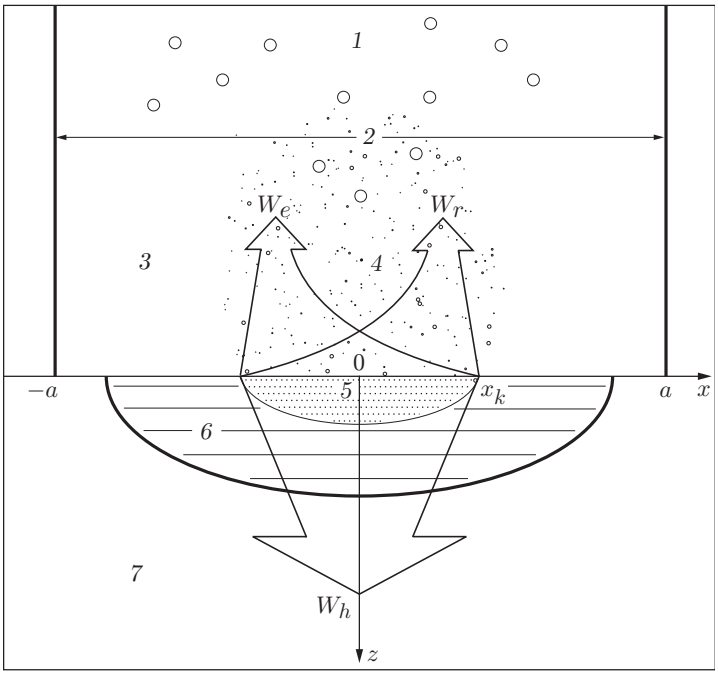


Fig. 1. Laser vaporization model: 1) nanoparticles; 2) laser beam; 3) gas; 4) vapor; 5) vaporization zone; 6) melt; 7) ceramics.

The object of the present work was to study the formation of nanoparticles by exposure of ceramic materials to continuous-wave $CO_2$ laser radiation of moderate power (up to 100 W) and to achieve an output sufficient for synthesis of nanomaterials for combinatorial catalysis.

During the study, it was required to find the optimum conditions of radiation–material interaction, to develop a technology for the preparation of the material being vaporized, and to determine the factors influencing the $CO_2$ laser parameters during synthesis of nanomaterials under laboratory conditions. Previous theoretical and experimental results on the interaction of laser radiation with materials are reported in [6–8].

The problem of laser synthesis of nanomaterials is split into five subproblems: 1) choice of a material and preparation of the starting samples (targets); 2) vaporization of the material by laser radiation in an atmosphere of an inert or reactive gas; 3) formation and transport of products from the vaporization zone; 4) entrapment of the nanoparticles and their size classification; 5) analysis of the products by physicochemical methods.

In the present study, emphasis was on the vaporization of materials by laser irradiation.

**1. Heating of a Dielectric Material by Laser Radiation.** In accordance with the established concepts [6–8] of the thermal nature of $CO_2$ laser irradiation of materials, we consider a three-dimensional axisymmetric problem of heating of a medium by radiation (Fig. 1). The material is at the bottom of Fig. 1, the laser radiation is incident from above, the gas flow direction coincides with the radiation propagation direction. Nanoparticles are synthesized by vapor condensation and coagulation in a gas flow, which carries the particles away from the high-temperature zone. In this zone there are the radiation-heated material, its melt, and the region of vaporization, whose characteristic depth is close to the radiation absorption length in the material. We assume that the vaporization front lags behind the melting front, but because the thermal conductivity of ceramic materials is lower than that of metals, the absorbed radiation energy remains near the melt zone. The temperature field in the sample is shown by isotherms that separate the boiling and melting zones. In the boiling zone there is absorption of the part of the radiation energy flux $W_a$ expended in heating of the sample ($W_h$), gray-law reradiation ($W_r$), and vaporization of the material ($W_e$). The quantity $W_e$ is defined by the formula

$$W_e = W_a - W_h - W_r. \tag{1}$$

To estimate $W_e$, we use the solution of the heat-conduction equation taking into account radiation absorption in the material is described by the Bouguer–Lambert law $I = I_0 \exp(-\alpha z)$. As a result, we obtain the following

temperature distribution $T$ in the target [8]:

$$T(x,z,t)=\frac{\alpha(1-R)P}{2c_p(2a)^2\rho}\int\limits_0^t\Big(\frac{\exp\left(-x^2/(a^2+4\chi\tau)+\alpha^2\chi\tau\right)}{1+4a^{-2}\chi\tau}\,F(z,\tau)\Big)\,d\tau+T_0,$$

$$F(z,\tau)=\exp\left(\alpha z\right)\operatorname{erfc}\left(\alpha\sqrt{\chi\tau}+z/\sqrt{4\chi\tau}\,\right)+\exp\left(-\alpha z\right)\operatorname{erfc}\left(\alpha\sqrt{\chi\tau}-z/\sqrt{4\chi\tau}\,\right).$$

Here $x$ and $z$ are the coordinates, $t$ and $\tau$ are time, $a$ is the Gaussian beam radius for the given focusing, $P$ is the incident-radiation power, $R$ is the coefficient of radiation reflection from the target surface, $\alpha$ is the radiation absorption coefficient, $\rho$ is the density of the target material, $c_p$ is the specific heat of the material, $\chi$ is the thermal diffusivity of the material, and $T_0$ is the initial temperature. It is assumed that the temperature field has axial symmetry and that the radiation is continuous in time and is incident normally to the surface. The material being heated is considered homogeneous. The temperature dependence of the material parameters $R$, $\alpha$, $\rho$, $c_p$, and $\chi$ is ignored. The action of the radiation begins at the time $t=0$.

Using the solution obtained, the time $t_\alpha$ required to heat the sample to the temperature $T_k$ at the center of the beam to the absorption depth ($x=0$ and $z=\alpha^{-1}$) is found from the relation

$$T(0,\alpha^{-1},t_\alpha)-T_k=0. \tag{2}$$

Here $T_k$ is the temperature at which the pressure of the saturated vapor of the material being vaporized is equal to the ambient gas pressure (boiling temperature). In this case, the absorbed energy is expended in heating of the sample. For any values of the parameters, if the temperature of the material does not reach the boiling temperature, Eq. (2) has no solution.

The radius of the boiling zone $x_k$ on the target surface at the time $t_\alpha$ is found from the equation

$$T(x_k,0,t_\alpha)-T_k=0.$$

The radius $x_k$ is smaller than the radius of the radiation focusing spot but is larger than the radiation absorption length $\alpha^{-1}$. In this case, the boiling zone can be represented as a cylinder. We find the total energy flux through the ends of the cylinder. The flux through the lateral surface is ignored since the height of the cylinder is much smaller than the radius of its base. The absorbed energy flux $W_a$ is equal to the product of the absorptivity $1-R$, the radiation power, and the geometrical efficiency of the energy contribution to the vaporization $\eta$, which is determined as the fraction of the power contained in the part of the Gaussian beam that falls in the boiling zone:

$$\eta=1-\exp\left(-x_k^2/a^2\right).$$

The energy flux $W_r$ reradiated by the boiling zone is given by the gray-body radiation law $W_r=\varepsilon\pi x_k^2\sigma T_k^4$, where $\varepsilon$ is the emissivity of the body and $\sigma$ is the Stefan–Boltzmann constant. The flux through the lower base $W_h$ that is expended in heating of the sample is considered equal to the product of the area of the base and the flux density at the center of the base: $W_h=-\pi x_k^2 k\,\partial T/\partial z$ ($k$ is the thermal conductivity; the derivative is calculated at the point $x=0$, $z=\alpha^{-1}$ at the time $t=t_\alpha$). The energy flux expended in vaporization is calculated by formula (1).

Let us find the radiation-energy utilization efficiency, which for the time $t_\alpha$ is defined as

$$\xi=W_e/P.$$

Figure 2 gives calculated curves of the geometrical efficiency of the energy contribution $\eta$ and the radiation-energy utilization efficiency $\xi$ versus the laser radiation intensity $I$ for an $Al_2O_3$ sample. The following parameter values were used: $P=85$ W, $R=0.05$, $\alpha=10^3$ cm$^{-1}$, $\varepsilon=0.4$, $\rho=1.5$ g/cm$^3$, $c_p=1.4$ J/(g$\cdot$ K), $\chi=5\cdot10^{-3}$ cm$^2$/sec, $T_0=300$ K, and $T_k=2800$ K (the value of $T_k$ corresponds to an ambient pressure equal to 0.05 atm [9]). From the curve of $\eta(I)$ it follows that for the above-mentioned calculation conditions, not more than 30% of the incident radiation power is absorbed in the boiling region. From Fig. 2, it also follows that as the $CO_2$ laser radiation intensity on the surface increases, the fraction of the energy (the upper-bound estimate) used for vaporization increases approximately from 5 to 15%. We note that in the calculation we ignored the heat of vaporization of the material, which influences the mass of the material being vaporized. However, despite the increase in the fraction of the energy used for vaporization, the mass of the material being vaporized may not increase because in the calculation we ignored variations in the thermal parameters of the medium and absorption

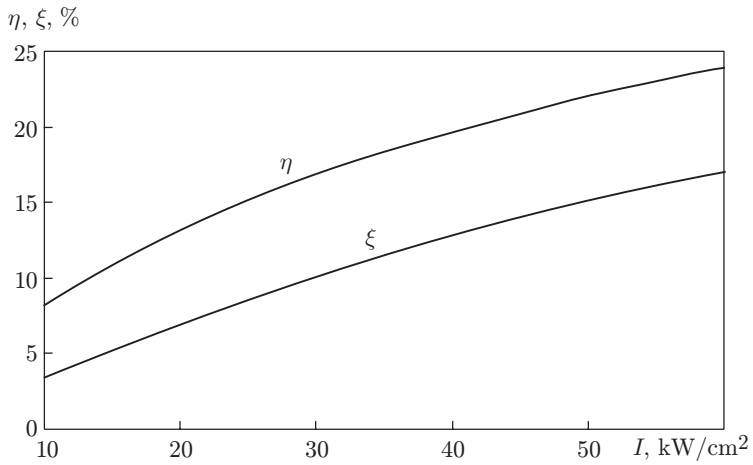


Fig. 2. Geometrical efficiency of the energy contribution to vaporization $\eta$ and the radiation utilization efficiency $\xi$ versus the radiation intensity $I$ on the target surface.

coefficient (which are insufficiently studied in the high-temperature region), the real three-dimensional geometry of the radiation–material interaction, and the finite scan rate.

For $\xi = 10\%$, $P = 85$ W, and the heat of vaporization and heating to the boiling temperature of 10 kJ/g, the output is 3 g/h. This estimate shows the possibility of vaporizing oxide materials by $CO_2$ laser radiation with a power of up to 100 W and a power density of $10^4$–$10^5$ W/cm$^2$, which is two orders of magnitude smaller than the boundary values for metals [2]. To attain the indicated power density in the far-field region, a $CO_2$ laser with an outlet aperture of 1 cm should have a diffraction divergence and time-stable radiation. The radiation reflected from the target should not have a significant effect on the laser generation conditions because of the presence of feedback. The facility should allow experiments to be performed over a broad range of carrier-gas pressures.

**2. Experimental Equipment and Samples.** A diagram of the experimental facility for producing nanomaterials by laser vaporization of targets is given in Fig. 3. The continuous-wave $CO_2$ laser designed and assembled by the authors has the following characteristics: radiation wavelength 10.6 $\mu$m, generation power up to 120 W on one $TEM_{00}$ transverse mode, output beam diameter 8 mm, divergence in the far-field region $3 \cdot 10^{-3}$ rad. The power is varied in the range $P = 10$–120 W. Power control is performed by a calibrated system consisting of a beam-splitting plate (made of ZnSe with an antireflection coating) and an LM-2 calorimeter (Karl Zeiss Jena, Germany).

Vaporization was performed in a vacuum chamber equipped with a radiation-focusing lens (a 135-mm focus KCl lens) and a rod brought outward for holding and scanning a cylindrical target by means of rotation with simultaneous movement along the rotation axis. In some cases, the sample was placed in a copper crucible fixed on the rod. A changeable FO paper filter of moderate porosity ("Blue ribbon" with a pore diameter of 3.0–3.5 $\mu$m) was placed at exit of the gas flow from the chamber. A labyrinth gas-flow path provided for separation of the debris emitted from the laser-irradiated target. Evacuation of the chamber and pumping of the gas from the container were implemented by two 2NVR-5DM backing pumps (Russia), which had a total output of 10 liters/sec. The pressure was monitored by a VO-11201 vacuum gauge (Russia).

The targets being vaporized had the shape of hollow cylinders of various heights with an outer diameter 14 mm, and an inner diameter of 6 mm. The $ZrO_2$ targets are produced by two methods:

1) dry pressing of a pure grade powder at a pressure of 10 MPa with the subsequent heating at a temperature of 800 °C for 4 h (the density of the samples was 2.4–2.6 g/cm$^3$);

2) deposition of zirconium hydroxide followed by mixing with an already dried hydroxide powder in a definite proportion and extrusion molding (the product pellets were dried first in air and then at a temperature of 110°C for 12–14 h and were then heated at a temperature of 1200°C for 4 h).

The $Al_2O_3$ targets were produced by the second method. For a number of targets, the heating temperature was maintained in the range from 800 to 1250°C. $LaNiO_3$ samples were prepared by dry pressing of the powder at

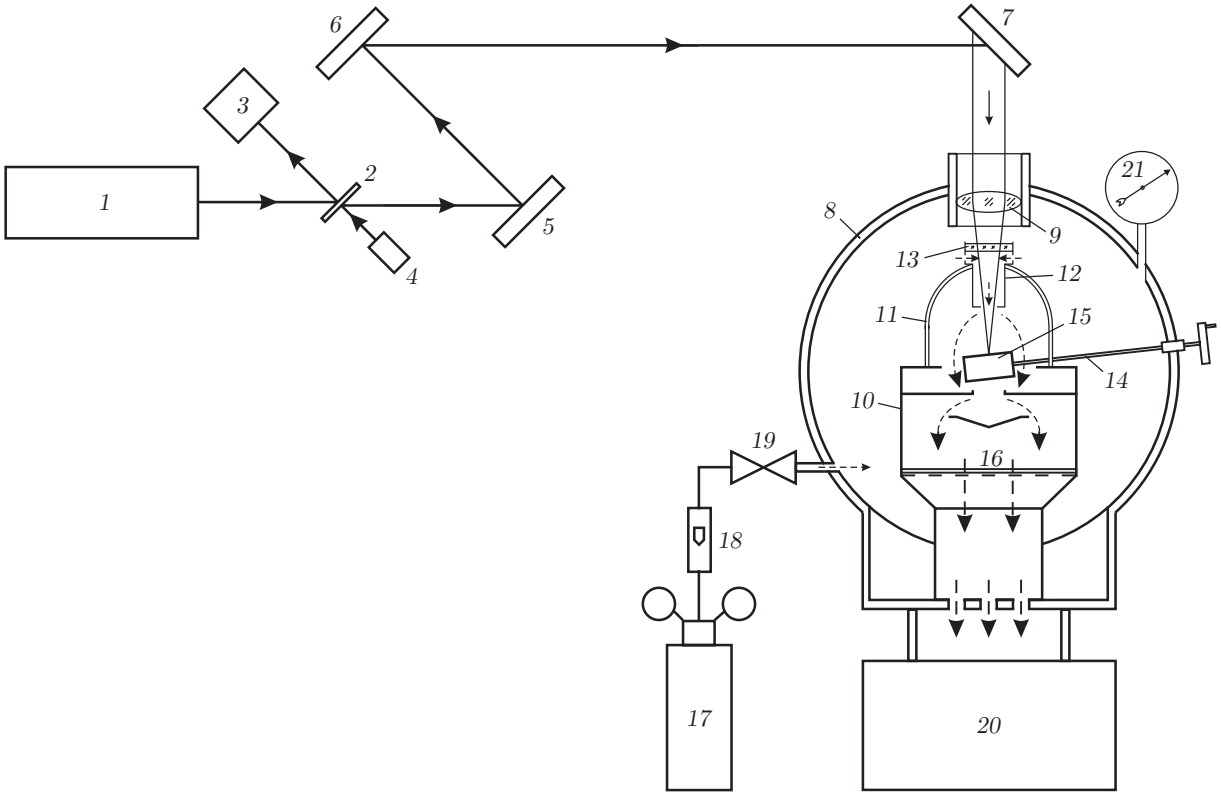


Fig. 3. Experimental setup: 1) $CO_2$ laser; 2) beam-splitting plate; 3) calorimeter; 4) tracing semiconductor laser; 5–7) optical track mirrors; 8) vacuum chamber; 9) lens; 10) vaporization chamber; 11) glass cap; 12) nozzle extension; 13) protective plate (KCl); 14) rod for holding and scanning the target; 15) target; 16) paper filter; 17) gas container. 18) rotameter; 19) valve; 20) gas-pumping system; 21) vacuum gauge; the solid arrows show the laser radiation direction; the dashed arrows show the gas flow direction.

a pressure of 12 MPa with the subsequent heating at a temperature of 300°C for 1 h. The density of the samples was 3.7 g/cm$^3$.

As the multicomponent material, we used the well-studied specimen — the Tsarev meteorite [10]. The catalytic activity of nanoparticles of its material has been determined in experiments.

The working gases were argon and helium. In most of the experiments, the chamber pressure was set in the range of 0.01–0.10 atm. The laser radiation power on the target surface was 75–85 W, and the power density was up to $5 \cdot 10^4$ W/cm$^2$. The rate of motion of the target surface relative to the beam was varied in the range of 0.1–10.0 cm/sec.

The mass of the nanomaterials produced was measured on a VLT-150-P electronic balance (Russia). X-ray powder analysis was conducted on a HZG-4 device (Germany). Electron-microscopic studies were performed on a JEM-2010 transmission electron microscope (JEOL, Japan) and a BS-350 scanning electron microscope (Tesla, Chechoslovakia). Specific surface area was measured by the Brunauer–Emmett–Teller (BET) method on a SORBI device (Russia) using nitrogen. The element composition was determined on a VRA-30 X-ray fluorometer (Germany) with a Cr anode. Laser-induced luminescence spectra were taken using a pulsed ArF laser with a wavelength of 193 nm on the spectroscopic facility of the Institute of Catalysis of the Siberian Division of the Russian Academy of Sciences [11].

**3. Experimental Results.** Vaporization parameters for $Al_2O_3$, $ZrO_2$, and $LaNiO_3$ samples in a helium atmosphere and the masses of the collected nanomaterials are given in Table 1.

Figure 4 shows an electron photomicrograph of the $Al_2O_3$ powder. Figure 5 gives a photograph of a section of the paper filter with a light precipitate of the $Al_2O_3$ powder. The diffraction pattern of the $Al_2O_3$ powder corresponded to an X-ray amorphous phase of the material — a highly dispersed disordered state of aluminum

TABLE 1

Vaporization Conditions

| Sample material | $\tau$, min | $p$, atm | $P$, W | $D$, mm | $v$, cm/sec | $M_*$, g |
|---|---|---|---|---|---|---|
| $Al_2O_3$ | 20 | 0.030 | 85 | 1.8 | 4.0 | 0,29 |
| $ZrO_2$ | 60 | 0.040 | 75 | 0.6 | 0.1 | 0.89 |
| $LaNiO_3$ | 30 | 0.006 | 75 | 2.0 | 0.1 | 1.50 |

**Note.** $\tau$ is the duration of experiment, $p$ is the gas pressure, $P$ is the radiation power, $D$ is the diameter of the radiation spot on the target, $v$ is the scan rate, and $M_*$ is the mass of the collected nanomaterial.

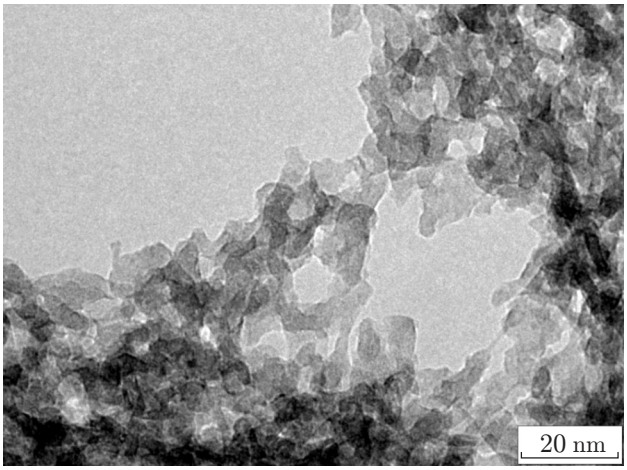


Fig. 4

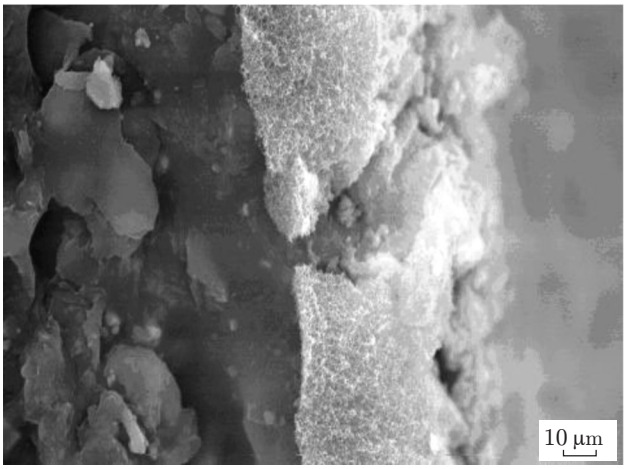


Fig. 5

Fig. 4. Aluminum oxide nanopowder.

Fig. 5. Section of the filter (on the left) with the nanopowder precipitate (on the right).

oxide. The size of the coherent scattering region determined by the line corresponding to line 440 of the $\gamma$-$Al_2O_3$ structure was 15 Å.

Figure 6 shows a photomicrograph of the $ZrO_2$ powder produced. The dependence of the characteristic particle size of the $ZrO_2$ nanopowder on the chamber pressure is given in Fig. 7. Particle size distribution histograms for $ZrO_2$ nanopowders produced at various pressures are shown in Fig. 8 ($m$ is the mass of particles of a definite fraction and $M$ is the total mass of the sample). The diffraction pattern of the $ZrO_2$ nanopowder exhibits not less than two phases: 1) monoclinic; 2) tetragonal or orthorhombic. It seems impossible to differentiate between the latter two phases because of their small particle sizes and similar phase parameters, and also because of the presence of the monoclinic phase. Others crystalline phases were not detected. The size of the coherent scattering region was 30 Å.

The specific surface areas $S_{\text{sp}}$ of $Al_2O_3$ and $ZrO_2$ samples produced in a helium atmosphere at various pressures $p$ are given in Table 2.

The results of X-ray fluorescence spectral analysis of the starting $LaNiO_3$ sample (target) and the remainder of the target after vaporization are given in Table 3.

Figure 9 shows laser-induced luminescence spectra of massive and nanodisperse (with a characteristic particle size of 5 nm) samples of the natural multicomponent material (the Tsarev meteorite). The element composition of the starting sample is given in Table 4.

**4. Discussion of Results.** The process of vaporization of the target by laser irradiation depends on the properties of the material, which are influenced by the sample preparation conditions. In some experiments with $Al_2O_3$ targets, visible sparks and debris emitted during irradiation. The smallest number of debris was formed in

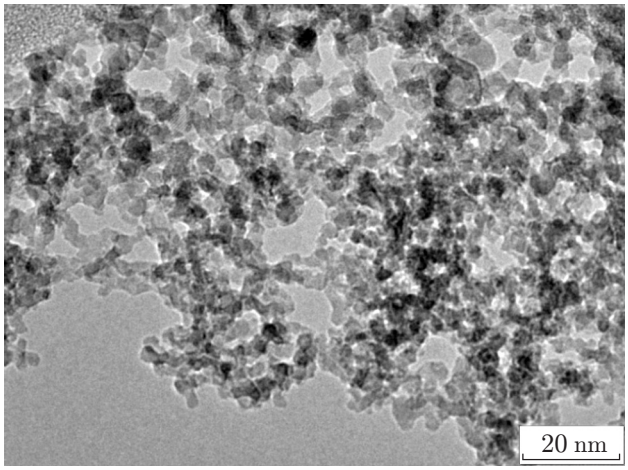


Fig. 6

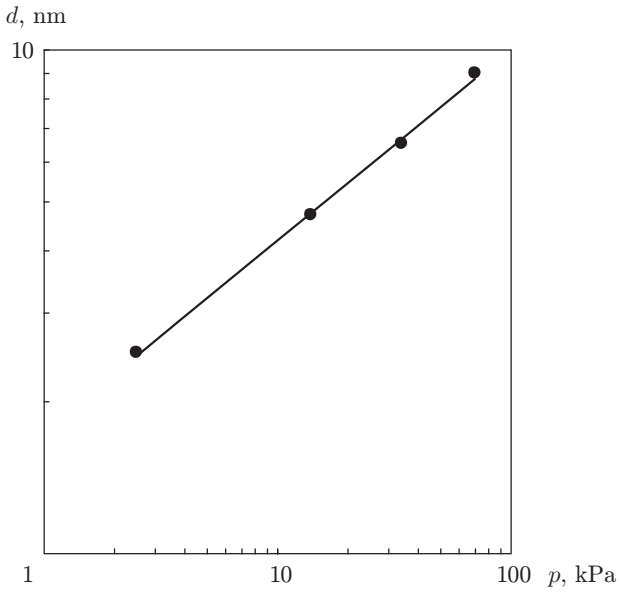


Fig. 7

Fig. 6. Zirconium oxide nanopowders.

Fig. 7. Characteristic particle size $d$ of $ZrO_2$ nanopowder versus pressure.

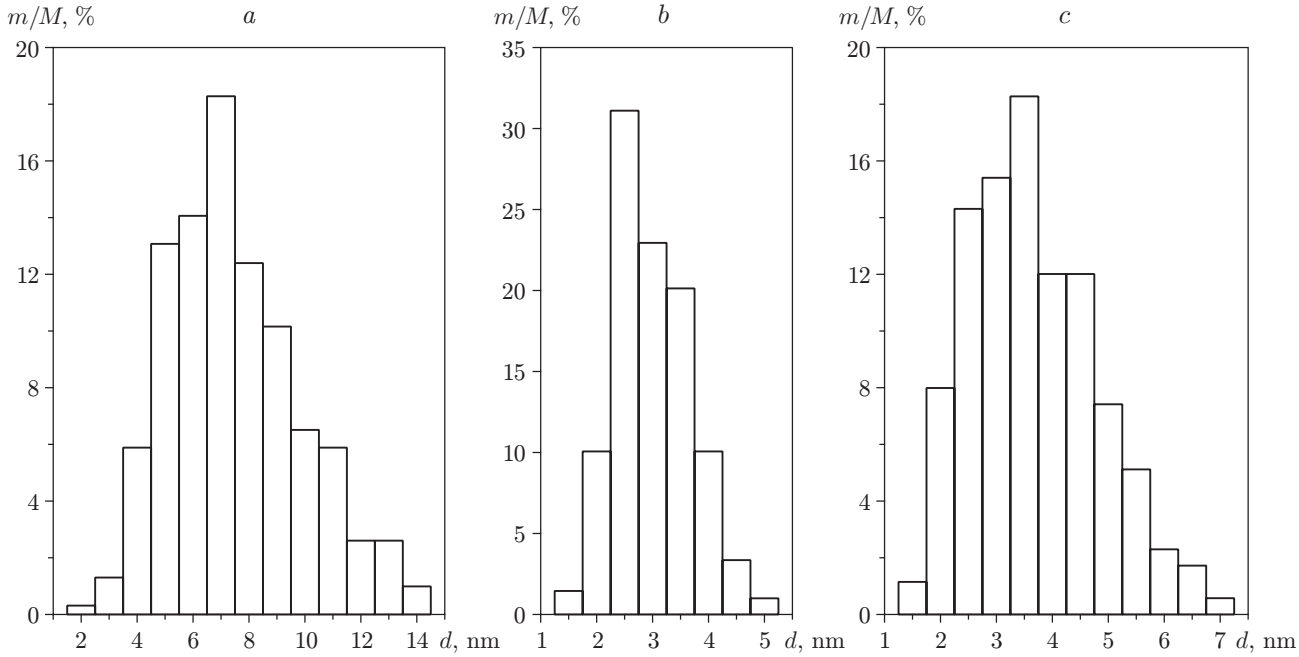


Fig. 8. Particles size distributions of $ZrO_2$ nanopowders produced for $p = 35$ (a), 2.5 (b), and 0.1 kPa (c).

TABLE 2

Specific Surface Area of the Samples Studied

| Sample material | $p$, atm | $S_{sp}$, $m^2/g$ |
|---|---|---|
| $Al_2O_3$ | 0.030 | 290 |
| | 0.060 | 404 |
| | 0.150 | 320 |
| $ZrO_2$ | 0.001 | 427 |
| | 0.025 | 307 |
| | 0.040 | 336 |

TABLE 3

Element Composition of the $LaNiO_3$ Target before and after Vaporization

| Sample analyzed | $g_{Ni}$, % | $g_{La}$, % |
|---|---|---|
| Starting sample (target) | 24.0 | 56.5 |
| Remainder of the target after vaporization | 3.5 | 47.0 |

**Note.** $g_{Ni}$ and $g_{La}$ are the mass fractions of Ni and La.

the case of dense targets ($\rho = 1.6$ g/cm$^3$) heated at a temperature of 1250°C. The targets having lower density fractured even at a low radiation intensity (approximately $10^3$ W/cm$^2$). This fracture could be due to the presence of atmospheric moisture, which was adsorbed in the pores of the target during storage and then vaporized under irradiation. Fracture occurred when the pore vapor pressure reached the strength limit of the sample. In the experiments with lower-density samples, a high scanning rate was required, which led to a considerable decrease in the output of the facility.

Performing experiments in two stages, with preliminary melting of the target surface by defocused radiation, made it possible to carry out the subsequent vaporization at lower rates of scanning of the target without deep burn through the sample.

For $Al_2O_3$ and $ZrO_2$ samples, the maximum output of the facility used for the synthesis of nanoparticles was 1 g/h. The smallest values of the specific radiation energy consumptions for the given samples were approximately 80 W$\cdot$ h/g. In the experiments, the laser energy utilization efficiency was determined as the ratio of the consumed radiation energy to the energy required to heat and vaporize the nanomaterial produced. Thus, to 300 kJ/g was expended to vaporize $Al_2O_3$ at the required energy of 10 kJ/g; i.e., the efficiency was 3%. This value remained constant in the intensity range $I = 10$–$57$ kW/cm$^2$ at a constant rate of motion of the target relative to the laser beam. High radiation power density, in turn, requires a high rate of scanning of the target surface and definite characteristics of the sample that should ensure fracture resistance under laser irradiation.

Vaporization from the crucible resulted in a factor of 2–3 decrease in the output compared to the results obtained for rotating cylindrical targets, which is explained by the impossibility of maintaining stable experimental conditions. The output achieved in an argon atmosphere was close to that in a helium atmosphere. However, in argon, the characteristic particle size of nanomaterials was several times larger than that in the experiments in helium and a broadening of the particle-size distribution was observed.

Vaporization of a number of multicomponent monolithic samples of minerals and the meteorite was performed using a crucible in a helium atmosphere at a pressure of approximately 0.05 atm, a power of 80 W, and a power density of $10^3$ W/cm$^2$. For most of the samples, the output was 0.5–1.0 g/h. A comparison of the laser-induced luminescence spectra of the starting material and the nanomaterial produced shows that the characteristic narrow lines of excited atoms are present in both spectra (see Fig. 9); therefore, the element compositions remained unchanged during the vaporization. In addition, for the nanodisperse sample at wavelengths of $\lambda = 260$ and 530 nm, broad luminescence bands are observed, which can be assigned to $SiO_2$ nanoparticles. From the results of X-ray fluorescence analysis, it follows that the mass fraction of metals is smaller in the product than in the starting material (see Table 3). Similar results were obtained in [3].

The results of experiments performed at various pressures showed that the characteristic particle size of and size distribution could be controlled. It was found, however, that a gas pressure decrease to $10^{-3}$ atm and a simultaneous decrease in the flow rate to 10 liters/h did not result in a further size reduction of the particles produced (see Fig. 8). The mean diameter of the product particles was 2–3 nm. Particles of smaller size were also present. Such particle sizes of the resulting powder meet the main requirements of catalytic technologies.

It should be noted that as the gas pressure decreases, a particle sizes reduction and a narrowing of the size distribution is accompanied by a decrease in the specific energy output of the process. This occurs because as the ambient gas pressure decreases, the saturated vapor pressure of the material being vaporized equal to the

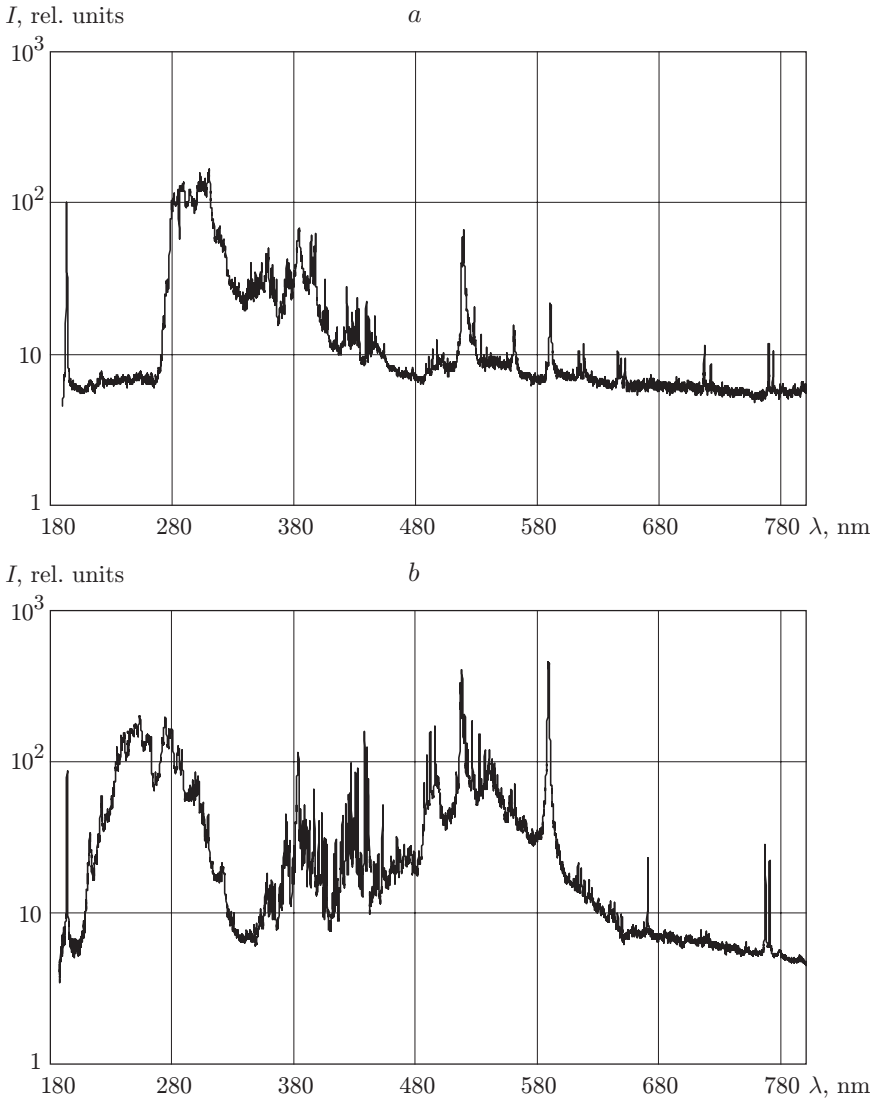


Fig. 9. Laser-induced luminescence spectra of the material of the Tsarev meteorite: a) starting basic material; b) nanomaterial.

TABLE 4

Element Composition of the Tsarev Meteorite [10]

| Element composition | $g$, % | Element composition | $g$, % | Element composition | $g$, % |
|---|---|---|---|---|---|
| $SiO_2$ | 40.58 | MnO | 0.34 | $P_2O_5$ | 0.30 |
| $TiO_2$ | 0.12 | MgO | 25.20 | Co | 0.048 |
| $Al_2O_3$ | 2.48 | CaO | 1.95 | Ni | 1.08 |
| $Cu_2O_3$ | 0.53 | $Na_2O$ | 0.67 | Cu | 0.013 |
| FeO | 13.98 | $K_2O$ | 0.096 | S | 1.92 |

ambient pressure is established at a lower temperature. For $Al_2O_3$, as the pressure decreases from 1 to $10^{-2}$ atm, the temperature of the establishment of the corresponding vapor pressure changes from 3250 to 2620 K [9].

The quantity of the nanomaterial collected on the filter depended on the gas flow rate through the vaporization chamber. For flow rates of about 10 liters/h and a pressure of $10^{-3}$ atm, the aerosol was almost entirely deposited on the walls of the vaporization chamber, i.e., the gas flow was insufficient to ensure effective transport of the particles and their deposition on the filter. As the gas flow rate was increased, the fraction of the material deposited on the filter increased. The flow rates were in the range of 150–200 liters/h, and the pressures in the range of 0.01–0.05 atm. Under these conditions, up to 70% of the total mass of the material being vaporized was deposited on the filter. Thus, under the indicated conditions, the transport of nanoparticles from the gas flow to the walls appears to occur by the diffusion mechanism.

Nanoparticles can pass through filter pores whose size far exceeds the nanoparticles diameter. However, as follows from the experiments, the fraction of the untrapped particles is minor. Particles can pass through the filter only in the initial stage of vaporization. This is supported by the fact that, first, the difference between the mass of the starting target and the overall mass of the target remainder after vaporization and the collected nanomaterials usually does not exceed 1% of the total mass of the nanomaterial produced; second, the nanopowder deposited on the paper filter forms a coat (see Fig. 5), which gradually builds-up and also begins to entrap nanoparticles.

Thus, effective vaporization of samples requires preliminary preparation of the material and creation of a sample with an optimal ratio of density (porosity) and thermal conductivity. The mean particle size of the nanopowder produced can be controlled by varying the pressure of the gas in which the vaporization is performed and by using gases with various molecular weights. The vaporization products are effectively removed from the high-temperature zone by blowing the gas above the target surface. To produce nanopowders that do not contain large particles resulting from fracture of the target, it is necessary to use an effective separation system. Filtration of the gas flow with nanoparticles through an obstacle with pore sizes of about 3 $\mu$m provides for effective collection of nanoparticles under the conditions of the experiments.

**Conclusions**. The calculations shows that during irradiation of ceramic targets by a continuous-wave $CO_2$ laser of moderate power (up to 100 W), not more than 15% of the laser radiation energy at a power density on the target of up to $10^5$ W/cm$^2$ can be expended in vaporization of the material. The rest of the laser radiation energy with a Gaussian cross-sectional intensity distribution is expended in heating of the target outside the focusing center. It is found experimentally that 3% of the entire radiation energy is used directly for the synthesis of nanoparticles by vaporization of aluminum oxide ceramics. The output of the experimental facility employed for the synthesis of nanodisperse powders of high-melting oxides is approximately equal to 1 g/h. The characteristic particle sizes are a few nanometers, which is appropriate for the solution of a number of modern problems related to the development and research of new nanomaterials.

We thank N. A. Rudina for electron-microscopic studies, V. A. Ushakov for X-ray studies of the samples, part of which was provided by V. A. Sadykov and N. M. Podgornykh (Tsaerv meteorite material).

This work was supported by the program on nanomaterials of the Presidium of the Russian Academy of Sciences and Integration project of the Siberian Division of the Russian Academy of Sciences No. 148.

## REFERENCES

1. P. P. Pescarmona, J. C. van der Waal, I. E. Maxwell, et al., "Combinatorial chemistry, high-speed screening and catalysis," *Catalys. Lett.*, **63**, Nos. 1/2, 1–11 (1999).
2. O. P. Solonenko, A. P. Alkhimov, V. V. Marusin, et al., *High Energy Processing of Materials* [in Russian], Nauka, Novosibirsk (2000).
3. Yu. A. Kotov, V. V. Osipov, M. G. Ivanov, et al., "Oxide nanopowders produced by vaporization of targets under pulsed $CO_2$ laser irradiation," *Zh. Tekh. Fiz.*, **72**, No. 11, 76–82 (2002).
4. D. B. Chrisey and G. K. Hubler (eds.), *Pulsed Laser Deposition of Thin Films*, John Wiley and Sons, New York (1994).
5. V. N. Snytnikov, A. S. Ivanova, E. M. Morozov, et al.,"Method of producing iron-containing oxide materials," Russian Patent No. 2158228 RU, C 01 G 49/00, Publ. 10.27.2000.

6. S. A. Anisimov, A. M. Prokhorov, V. E. Fortov, et al., "Use of high-power lasers in studies of materials at ultrahigh pressures," *Usp. Fiz. Nauk*, **142**, No. 3, 395–434 (1984).
7. J. F. Ready, *Effects of High-Power Laser Radiation*, Academic Press, New York (1971).
8. N. I. Koroteev and I. L. Shumai, *Physics of High-Power Laser Radiation* [in Russian], Fizmatlit–Nauka, Moscow (1991).
9. I. K. Kikoin (ed.), *Tables of Physical Quantities: Handbook* [in Russian], Atomizdat, Moscow (1976).
10. L. D. Barsukova, V. Ya. Kharitonova, and L. N. Bannykh, "Chemical composition of the Tsarev meteorite," *Meteoritika*, No. 41, 41–43 (1982).
11. V. N. Snytnikov, V. O. Stoyanovskii, K. S. Raspopin, and V. N. Parmon, "Laser-induced luminescence of oxide catalysts excited by ArF laser radiation," *Dokl. Ross. Akad. Nauk*, **392**, No. 4, 501–505 (2003).